Opposing modulation of Cx26 gap junctions and hemichannels by CO_2

Sarbjit Nijjar[1], Daniel Maddison[1], Louise Meigh[1], Elizabeth de Wolf[1], Thomas Rodgers[2], Martin Cann[3], Nicholas Dale[1]

[1]School of Life Sciences
University of Warwick
Coventry
CV4 7AL

[2]School of Chemical Engineering and Analytical Science
University of Manchester
Oxford Road
Manchester
M13 9PL

[3]Department of Biosciences
Durham University
Stockton Road
Durham
DH1 3LE

Abstract

Cx26 hemichannels open in response to moderate elevations of CO_2 (PCO_2 55 mmHg): CO_2 reversibly carbamylates Lys125, and the resulting carbamate forms a salt bridge to Arg104 of the adjacent subunit biasing the hemichannel to the open state. Here we show that CO_2 closes the Cx26 gap junction via a mechanism that also depends on both Lys125 and Arg104. Our mutational analysis shows that pH-dependent and CO_2-dependent closure of the gap junction are mechanistically independent. Mutations of Cx26 associated with Keratitis Ichthyosis Deafness syndrome that remove CO_2 sensitivity from the hemichannel, also abolish the CO_2-dependent gap junction closure. Elastic network modelling suggests that the lowest entropy state, when CO_2 is bound, is in the open configuration for the hemichannel and the closed configuration for the gap junction. Surprisingly, we conclude that the opposing actions of CO_2 on Cx26 gap junctions and hemichannels results from carbamylation of the same residues.

Introduction

The canonical function of connexins is to form intercellular junctions between cells –gap junctions – through the docking of hexameric connexons in the opposing membrane of each cell. However, the individual connexons –known as hemichannels –can also function on their own (Huckstepp et al., 2010b; Pearson et al., 2005; Stout et al., 2004; Weissman et al., 2004). Hemichannels act as plasma membrane channels, which in addition to mediating transmembrane ionic currents, also permit the transmembrane fluxes of small molecules such as ATP (Huckstepp et al., 2010a; Kang et al., 2008; Pearson et al., 2005; Stout et al., 2002).

We have studied the hemichannels of connexin26 (Cx26) and found that these hemichannels are directly gated by CO_2 (Huckstepp et al., 2010a; Meigh et al., 2013; Meigh et al., 2014). CO_2 opens the hemichannel and permits the efflux of ATP, which can act as a neurotransmitter. This is particularly important in the CO_2 sensitive control of breathing where Cx26 hemichannels in the medulla oblongata act as novel chemosensory transducers (Huckstepp and Dale, 2011; Huckstepp et al., 2010a). The action of CO_2 on Cx26 occurs via carbamylation of the residue K125. The carbamylated lysine forms a salt bridge to R104 of the neighbouring subunit (Figure 1a). These intersubunit carbamate bridges bias the hemichannel to the open configuration (Meigh et al., 2013). Extensive evidence supports a direct action of CO_2 on the hemichannel rather than an indirect effect via pH: 1) in isolated inside-out or outside-out patches changes in PCO_2 at constant pH alter Cx26-gating (Huckstepp et al., 2010a); 2) insertion of the carbamylation motif into Cx31, which is insensitive to CO_2, creates mutant Cx31 hemichannels that can be opened by CO_2 (Meigh et al., 2013); 3) mutation of the key residues K125 and R104 to respectively arginine and alanine destroys

CO_2-sensitivity of the hemichannel; 4) the mutations K125E and R104E (in effect engineering the action of CO_2 into the subunit via the carboxy group of glutamate) create constitutively open hemichannels which are CO_2-insensitive (Meigh et al., 2013); 5) the mutation K125C creates a hemichannel that can be opened with NO or NO_2 via a nitrosylation reaction on the cysteine residue at 125 and subsequent salt bridge formation to R104 (Meigh et al., 2015); and 6) the double mutation K125C and R104C creates a redox-sensitive hemichannel presumably via disulfide bridge formation between the cysteine residues at 104 and 125 (Meigh et al., 2015).

Although the actions of CO_2 on Cx26 hemichannels are well characterized, we have not studied the action of CO_2 on Cx26 gap junctions. When the two connexons dock to form a complete gap junction, there is likely to be significant conformational rearrangement and constraint of the resulting dodecameric complex. Therefore, we cannot assume that CO_2 will modulate a complete gap junction in the same way as a hemichannel. There has been a previous study on the closing effect of CO_2 on Cx32 and Cx26 gap junctions expressed in *Xenopus* oocytes (Young and Peracchia, 2004). This prior study used non-physiological conditions in which both the extracellular and intracellular pH would become very acidic: exposure to 30-100% CO_2 in the absence of bicarbonate in the extracellular medium. This study most likely reported an effect of pH on the gap junction. In this paper, we report the actions of physiological concentrations of CO_2, in a CO_2/HCO_3^- buffered system at constant extracellular pH, on gap junctions formed between pairs of HeLa cells expressing Cx26. To our surprise, we find that modest increases in PCO_2 *close* complete gap junctions, and that this is most likely a direct effect mediated through its binding to the same residues that result in the *opening* of the hemichannel. This result reinforces the need to develop further high-resolution structures for Cx26 hemichannels and gap junctions with and without CO_2 bound.

Results

Our extensive prior studies on the parental HeLa cells show them to be devoid of Cx26, and of any other type of CO_2-sensitive hemichannel. (Huckstepp et al., 2010a; Meigh et al., 2013; Meigh et al., 2014).

To study gap junctions, we made simultaneous whole cell recordings from isolated pairs of Cx26-expressing HeLa cells that were in close contact. These cells had a high probability of being electrically coupled. On establishing whole cell recordings from each cell, the cells were clamped at a holding potential of -50 mV. We used a simple protocol of repeated 10 mV steps, alternating in each cell, to measure both the whole cell conductance of each cell and the junctional conductance between the cells (Figure 2a). In all the illustrations, the outward currents during the voltage steps are a measure of the whole cell conductance, and the inward currents during the voltage steps are

proportional to the junctional conductance. Parental cells could exhibit gap junction coupling but this was insensitive to CO_2 (Figure 2b, summary statistical data in Figure 7a).

Cx26 Gap junctions are closed by CO_2

Under control conditions (PCO_2 35 mmHg), Cx26 gap junctions had a linear current voltage relation (Figure 2c). This linearity was retained but the slope of the relationship was greatly reduced during application of hypercapnic saline (PCO_2 55 mmHg) at a constant extracellular pH of 7.5. As CO_2 had an apparently identical effect at all transjunctional voltages tested, this supports the use of the simple protocol outlined in Figure 2a to test the CO_2 sensitivity of Cx26 gap junctions. In every case we found that the CO_2 stimulus caused a reduction of junctional coupling (Figure 3). In some cases, this was a partial effect and, in other cases, the Cx26 gap junctions were completely closed. Overall the median change of the Cx26 gap junction conductance (from control to CO_2 stimulus) was -5.6 nS (95% confidence limits -11.9 and -3.2 nS, *n*=29). We also observed that the effect of CO_2 was sometimes reversible (16/29 cases, Figure 3a, b), and on other occasions irreversible within the duration of the whole cell recordings (13/29 cases, Figure 3c). This contrasted with the rapid reversibility of the effect of CO_2 on the hemichannel opening (Figure 3c).

Using the protocol of Figure 2a, we measured both the whole cell conductance and the junctional conductance. As the junctional conductance was reduced by CO_2, we would also expect the whole cell conductance to reduce simultaneously, as the gap junction represents a current path out of the cell. We did indeed observe parallel reductions of the whole cell and junctional conductances (e.g. Figure 3b). However, in some cases the whole cell conductance did not reduce appreciably despite a reduction in the junctional conductance (e.g. Figure 3a, c), suggesting that a parallel increase in whole cell conductance may have masked the expected reduction. This is most easily explained if the pairs of HeLa cells express both Cx26 hemichannels and gap junctions; the simultaneous opening of Cx26 hemichannels and closure of gap junctions would partially mask any reductions of net whole cell conductance. To assist interpretation of the electrophysiological recordings from HeLa cells that had variable proportions of hemichannels and gap junctions, which are oppositely modulated by CO_2, we developed a simplified model of the currents and their modulation by CO_2 in each of the coupled cells (Figure 4). The three panels in Figure 4 give calculated examples that correspond to the equivalent three panels in Figure 3.

Our results lead to the surprising observation that CO_2 has opposite effects on Cx26 gap junctions and hemichannels. Not only does CO_2 close gap junctions in contrast to opening hemichannels, this closure of the gap junction appears to be more slowly reversible, at least in some cases, than the modulation of the hemichannel.

Permeability to fluorescent dyes shows CO_2-dependence

To verify our patch clamp results by an alternative approach, we studied the CO_2-sensitivity of permeation of a fluorescent glucose analogue (2-Deoxy-2-[(7-nitro-2,1,3-benzoxadiazol-4-yl)amino]-*D*-glucose, NBDG) through the gap junctions formed between HeLa cells stably, or transiently expressing Cx26. Whole cell recordings were made from a single cell in a coupled pair or group. NBDG was introduced, via the patch pipette, into a single cell (the *donor*) of a coupled pair, and the time taken for the dye to diffuse into a coupled cell and achieve 10% of the fluorescence intensity of the donor cell was determined (Figure 5a). We performed this assay under two conditions -starting in solutions with a PCO_2 of 35 mmHg, and then in cells where the PCO_2 started at 55 mmHg and was then swapped after 2 minutes to a PCO_2 of 35 mmHg. In cells that started with a low PCO_2 the NBDG permeated into the coupled cells rapidly (Figure 5b, c). However, when the recording was initiated in saline with a PCO_2 of 55 mmHg, there was little permeation during the period of high PCO_2 and this only occurred once the PCO_2 was reduced to 35 mmHg (Figure 5b). As a result, the time taken for the fluorescence to reach 10% of the donor cell was much longer than when the recordings were initiated in low PCO_2 (Figure 5c).

CO_2 acts directly on the gap junction

In studying the direct modulation of Cx26 hemichannels by CO_2 we identified two key residues in the carbamylation motif, K125 and R104, that are required for CO_2-dependent opening of the hemichannel (Meigh et al., 2013). We also established that hemichannels of Cx31, which lack the carbamylation motif, were insensitive to CO_2 (Meigh et al., 2013). We made recordings from pairs of Cx31 expressing HeLa cells and found that neither the whole cell conductance, nor the gap junction conductance were altered by application of hypercapnic saline (Figures 6, 7a; median change in conductance 0.07 nS, 95% confidence limits 0.44 and -0.29 nS, n=12). This suggests that the carbamylation motif is required for CO_2-dependent closure of gap junctions.

To further test the requirement of the carbamylation motif, we studied the mutation K125R, which removes the CO_2 sensitivity of Cx26 hemichannels (Meigh et al., 2013). This is because Arg is more basic than Lys and therefore cannot be carbamylated by CO_2. We found that gap junctions formed between HeLa cells expressing $Cx26^{K125R}$ were insensitive to CO_2 (Figures 6, 7a; median change in conductance 0.01 nS, 95% confidence limits 0.2 and -0.06 nS, n=14).

We used NBDG transfer to verify that the K125R mutation abolished the CO_2-dependent closing of Cx26. Our data showed that unlike wild type Cx26 gap junctions, CO_2 made no difference to the rate

of dye transfer between cells coupled via $Cx26^{K125R}$ (Figure 7b). We next tested whether the mutation R104A, which also removes CO_2 sensitivity from Cx26 hemichannels (Meigh et al., 2013), affected the CO_2 sensitivity of Cx26 gap junctions. CO_2 made no difference to the rate of NBDG transfer between cells coupled via $Cx26^{R104A}$ (Figure 7b).

Our results therefore suggest the important conclusion that Cx26 gap junction closure by CO_2 depends upon the same residues (K125 and R104) that are required for hemichannel opening by CO_2. This in turn suggests that the gap junction closure is mediated via the same carbamylation mechanism that opens hemichannels.

Mutation of the carbamylation motif does not alter pH sensitivity of the gap junction

Gap junctions can be closed by acidification. We therefore tested whether intracellular acidification by application of 30 mM propionate (Haussig et al., 2008; Jahromi et al., 2002) could close the Cx26 gap junction, and whether this could be altered by the K125R mutation, which eliminates CO_2 dependent closure. We found that the propionic acid treatment reduced the gap junction conductance of wild type Cx26 by 5.3 nS (median, 95% Confidence limits 2.8 and 8.3 nS, n=12). This manipulation also reduced the gap junction conductance of $Cx26^{K125R}$ by a similar amount 7.7 nS (median, 95% Confidence limits 4.1 and 11.0 nS, n=13, Figure 8). We therefore conclude that the actions of CO_2 and pH on Cx26 gap junctions are independent, and that the pH induced gap junction closure does not require the carbamylation motif.

Effect of KID syndrome mutations on CO_2-dependence of gap junction coupling

We have previously shown that KID syndrome mutations A88V, N14K, and A40V (Figure 1) abolish the ability of CO_2 to open the mutant hemichannels (Cook et al., 2019; de Wolf et al., 2016; Meigh et al., 2014). Recently, we discovered that certain KID syndrome mutations induce alternative splicing of the Cx26 mutation when this is tagged with a fluorescent protein (Cook et al., 2019). This splicing results in poor expression and cell death can be prevented by also mutating the 5' splice site (Cook et al., 2019). However, the 5' splice site cannot be silently mutated so we chose a conservative mutation, M151L (Figure 1), which appeared to have little effect on Cx26 expression by itself. $Cx26^{M151L}$ hemichannels are blocked normally by extracellular Ca^{2+} and they retain CO_2-sensitivity (Cook et al., 2019). Furthermore, $Cx26^{A40V,M151L}$ hemichannels are insensitive to CO_2 (Cook et al., 2019). However, the mutation M151L is a rare allele associated with non-syndromic hearing loss (Siemering et al., 2006).

As we wished to exploit the ability of M151L to prevent the alternative splicing of the KIDS mutated Cx26, we first examined whether $Cx26^{M151L}$ permitted gap junction formation. Gap junction structures were clearly visible (Supplementary Figure 1a). However, in 47 different recordings we did not observe either dye coupling (Supplementary Figure 1b) or the electrophysiological hallmarks of electrical coupling (slowed capacitive charging currents during a voltage step indicative of current flow through the gap junction). By contrast, cells expressing $Cx26^{A40V,M151L}$, $Cx26^{A88V,M151L}$ and $Cx26^{N14K,M151L}$ exhibited dye coupling in 14/15, 12/12 and 12/12 recordings respectively. These frequencies of coupling are statistically different χ^2 = 82.2 (3 degrees of freedom, p=5.1 x 10^{-18}). Surprisingly, we conclude that the mutation M151L prevents permeation through gap junctions that are apparently formed but either remain closed at the transjunctional potential studied here, or are otherwise non-functional.

When the M151L mutation was combined with the KIDS mutations, A40V, A88V or N14K, in each case, the doubly mutated Cx26 was invariably capable of forming functional gap junctions through which NBDG could permeate (Figure 9). The KIDS mutations appear to compensate for the deficiency in gap junction permeability introduced by the M151L mutation. For all three mutations, the Cx26 gap junction remained open in the presence of 55 mmHg PCO_2 (Figure 9), a concentration that would normally close the wild type gap junction. Thus, the KIDS mutations not only prevent CO_2-dependent opening of the hemichannel, but also prevent CO_2-dependent closing of the gap junction, at least when combined with M151L. Interestingly, the effect of N14K on hemichannel sensitivity to CO_2 is less than the other KIDS mutations (de Wolf et al., 2016) and this parallels the trend in our data that permeation of NBDG through the $Cx26^{N14K,M151L}$ gap junctions, while still occurring, may be slightly slowed at the higher level of PCO_2 (Figure 9c, d).

Elastic network modelling

Previous experimental data points to the importance of carbamylation of K125 and the formation of a salt bridge to R104 in the adjacent subunit to facilitate Cx26 hemichannel opening in response to CO_2. It is not clear from this mechanism alone why the dodecameric Cx26 gap junction would be closed by CO_2. Previous work has used coarse-grained modelling to demonstrate a mechanism whereby CO_2 constrains the Cx26 hemichannel in the open state (Meigh et al., 2013). We therefore used further coarse-grained modelling to probe the difference in behaviour of the Cx26 hemichannel and gap junction. Coarse-grained modelling reduces protein atomistic complexity for efficient computational studies of harmonic protein dynamics and is particularly suited to examining the contribution of entropy to channel opening over millisecond time scales (Sherwood et al., 2008). While it is not possible to be certain that such calculated dynamics are true in the absence of experimentally determined structures, coarse-grained modelling has helped to support and explain

structural data for membrane protein conformational changes (Isin et al., 2012; Sherwood et al., 2008; Shrivastava and Bahar, 2006; Zheng and Auerbach, 2011).

In an Elastic Network Model (ENM) the Cα-atom coordinates of an atomic resolution structure are used to represent a protein structure. Global protein harmonic motions within the ENM consists of a defined number of modes, each of a characteristic frequency and representing a particular harmonic motion within the protein. ENMs reproduce protein global low frequency modes well in comparison to experimental data (Delarue and Sanejouand, 2002; Valadie et al., 2003). We therefore built coarse-grained ENMs (Tirion, 1996) to gain insight into the mechanism by which CO_2 maintains the Cx26 hemichannel in the open state but the Cx26 gap junction in the closed state. ENMs were constructed using the coordinates from high-resolution crystal structures for the Cx26 hemichannel and gap junction in the CO_2 unbound state. CO_2 was represented in the ENMs by the inclusion of additional Hookean springs between residues K125 and R104 of neighbouring monomers in both the hemichannel and the gap junction (Meigh et al., 2013).

We examined the similarities between eigenvectors for the Cx26 hemichannel and gap junction to understand the changes in harmonic protein motion caused by CO_2-binding. The main open-close mode in the Cx26 hemichannel is defined as the lowest frequency mode that ignores the solid body translational and rotational motions. The solid body translational and rotational motions consist of six modes and so the open-close mode is mode 7 (Meigh et al., 2013). This open-close mode in the hemichannel in the absence of CO_2 (mode 7) becomes reordered as mode 15 in the presence of CO_2 (Figure 10a; red-bordered square). The main open-close mode in the gap junction in the absence of CO_2 (mode 10; modes 7-9 represent motions between the two hexamer rings) becomes reordered as mode 24 in the presence of CO_2 (Figure 10b; green-bordered square). Analysis of the overlap between the main open-close mode in the gap junction and hemichannel in the absence of CO_2 reveals an almost complete overlap between mode of the hemichannel (mode 7) and the gap junction (mode 10) (Figure 10c, blue-bordered square). The basic open-close dynamics are therefore likely similar between gap junction and hemichannel.

To understand the differing roles of CO_2 in the hemichannel and gap junction, we calculated a range of partially open and closed eigenvectors for both the hemichannel and the gap junction. We then calculated at each state, for both the hemichannel and gap junction, the free energy for CO_2-binding and the influence of CO_2 on the open/close eigenvector. This calculation provides a free energy for each state examined along the open/close eigenvector. Calculation of the free energy difference between the CO_2-bound and unbound state provides information on the stability (binding energy of CO_2 needed) for each state. In this case, the closer the value is to zero, the less energy needed to bind CO_2 (Figure 10d). The *x*-axis of the Figure represents trajectory along the open/close

eigenvector where the higher the value the more closed the hemichannel or gap junction. The *y*-axis of the Figure represents the difference in free energy for the CO_2-bound and non-bound state where the higher the value is hypothesised to be less preferable for CO_2-binding. On binding CO_2 the hemichannel (6mer) or gap junction (12mer) will progress along the open/close eigenvector to make the difference in free energy more favourable for the CO_2-bound state.

For the hemichannel, it is energetically favourable to bind CO_2 in the open-state and then energetically unfavourable to close. For the gap junction it is energetically favourable to bind CO_2 in the closed state and then energetically unfavourable to open. The differences in the open/closed state of the gap junction and hemichannel in response to CO_2 can therefore be explained through entropy contributions to free energy change.

Discussion

The key result from our study is that Cx26 gap junctions and hemichannels are modulated in an opposing manner by CO_2. CO_2 closes the gap junction but opens the hemichannel. Of note, these diametrically opposite actions of CO_2 on gap junctions and hemichannels depend on the same residues and presumably the same carbamate bridging mechanism.

Opposing modulation of gap junctions and hemichannels has been reported before. LPS and bFGF inhibit Cx43 gap junctions and open Cx43 hemichannels. While apparently similar to the results reported in this study, the modulation of these two entities is downstream of kinase activity and the signaling actions of arachidonate metabolites; i.e. these are indirect effects on Cx43 and are unlikely to involve the same residues in the protein (De Vuyst et al., 2007). Similarly, the cytokines IL1β and TNFα also inhibit Cx43 gap junctions and open Cx43 hemichannels (Retamal et al., 2007a). Both of these effects are mediated through a p38 MAPK dependent pathway. However, hemichannel opening triggered by these cytokines is sensitive to inhibition of nitric oxide synthase or changing redox state (Retamal et al., 2007b), whereas the gap junction closure is insensitive to redox state. Thus for the two entities, the mechanisms of modulation evoked by the p38 MAPK pathway differ (Retamal et al., 2007a).

Implications for structural biology of Cx26

The crystal structure of Cx26 shows the molecule in the form of a gap junction (Maeda et al., 2009). The two connexons dock via interactions involving the two extracellular loops (E1 and E2) of each subunit. There are multiple hydrogen bonds formed between the opposing E1 and E2 loops of each connexon (Maeda et al., 2009). These give a tight interaction that is likely to alter and constrain the

conformation of hemichannels docked in a gap junction versus undocked hemichannels. The opposing modulation of gap junctions and hemichannels by CO_2 must presumably arise from the conformational differences between free versus docked hemichannels.

Our ENM calculations of the interaction of CO_2 with Cx26 hemichannels uses the docked hemichannel from the gap junction as a model for the structure of the free hemichannel (Meigh et al., 2013). This model allowed us to propose a plausible gating mechanism for CO_2-dependent opening of the hemichannel, which we have supported with extensive mutational analysis (Meigh et al., 2013). We exploited this knowledge to introduce novel gating mechanisms via the same intersubunit interactions by mutating Lys125 to Cys (Meigh et al., 2015). This made the hemichannel NO-sensitive, via nitrosylation of the Cys125 and interaction with Arg104 of the neighbouring subunit. The double mutation -K125C, R104C - made the hemichannel redox sensitive (via redox modulation of disulfide bridges between subunits) (Meigh et al., 2015). The mutated residues in these Cx26 variants are some considerable distance apart –far further than the short distances normally required for the ionic and covalent interactions between the respective residues. That these mutations were nevertheless effective at changing the gating of Cx26 implies considerable flexibility of the hemichannel that can bring apparently distant residues close enough to interact (Meigh et al., 2015).

Despite this success in using a half gap junction as a model for the free hemichannel, the results in this study suggest the need for considerable caution in any future structural modeling of hemichannels. Not only may the isolated hemichannel be far more flexible than a hemichannel that is part of a gap junction, but it may also have a substantially different conformation. New structures of Cx26 hemichannels and gap junctions are therefore needed to probe their conformational differences, and provide firm mechanistic understanding of the differential modulation of hemichannels and gap junctions by CO_2.

Reversibility

CO_2 carbamylation of primary amines is a highly labile and reversible covalent interaction (Lorimer, 1983). We would therefore expect closure of the gap junction by CO_2 to be readily reversible. Our dye transfer experiments clearly show that gap junction closure reverses (Figure 5 and 7), but we did not always observe this with patch clamp recording (e.g. Figure 3c). This variable reversibility in the patch recordings is most likely due to the technical limitation of making stable recordings from flat cells for long periods rather than any fundamental property of the modulation by CO_2. Nevertheless, the closure of the Cx26 gap junction appeared to reverse more slowly than the opening of Cx26 hemichannels. There are six potential binding sites for CO_2 in the Cx26 hemichannel. The Hill coefficient for the effect of CO_2 on the hemichannel has been estimated

between 4-6 (de Wolf et al., 2017; Huckstepp et al., 2010a), suggesting that several CO_2 molecules may be required to bind to open the hemichannel. For the complete gap junction there are 12 possible binding sites for CO_2. While we do not know how many molecules of CO_2 need to bind to close Cx26 gap junctions, or whether there might be cooperativity involved in CO_2 binding, it is possible that if all 12 binding sites were occupied, the resulting structure might be in a relatively stable closed configuration that would require significant time to reverse.

Independence of pH and CO_2 dependent modulation of Cx26 gap junctions

We find that the carbamylation motif in Cx26 is required for both the CO_2-dependent opening of hemichannels and the CO_2-dependent closure of gap junctions. The link between the CO_2-dependent modulation of hemichannels and gap junctions is not immutable. Cx26 hemichannels of the lung fish *Lepidosiren* are insensitive to CO_2, yet their gap junctions are still closed by CO_2 (Dospinescu et al., 2019). The contrary case is demonstrated by Cx32: hemichannels of this connexin can be opened by CO_2, but Cx32 gap junctions are insensitive to the same doses of CO_2 (Dospinescu et al., 2019). Our finding that direct manipulation of intracellular pH will still close $Cx26^{K125R}$ gap junctions, demonstrates that the pH dependent and CO_2 dependent closure of this gap junction are mechanistically independent. This is also true for the effects of CO_2 and pH on hemichannels, because acidification causes hemichannel closure (Yu et al., 2007), whereas an increase in PCO_2 causes hemichannel opening (Huckstepp et al., 2010a).

KIDS mutations and Cx26 gap junctions

There are relatively few reports of the effects of KIDS mutations on Cx26 gap junctions. Prior reports suggest that the A40V mutation prevents Cx26 gap junction formation (Montgomery et al., 2004). Clearly our data suggest that, in HeLa cells and in combination with the mutation M151L at least, the A40V mutation does not prevent formation of functional gap junctions (Figure 9a). Our data suggests further that N14K and A88V KIDS mutations (once again in combination with M151L) do not prevent gap junction formation and that these gap junctions are highly permeable to NBDG.

KIDS mutations are thought to cause the syndrome through gain-of-function. Several lines of evidence suggest that KIDS mutated Cx26 hemichannels are leaky: either they are less sensitive to Ca^{2+} blockade (Lopez et al., 2013; Mese et al., 2011; Sanchez et al., 2014; Sanchez et al., 2010; Zhang and Hao, 2013) or have an altered voltage sensitivity such that they spend more time in the open state at transmembrane potentials closer to the resting potential (Sanchez et al., 2016; Valdez Capuccino et al., 2019). Our finding that three KIDS mutations studied here prevent gap junctions from closing to CO_2 is effectively a further gain of function caused by these mutations: they will

remain open under conditions of elevated CO_2. Interestingly, A40V hemichannels in oocytes are less sensitive to pH blockade than wild type Cx26 hemichannels, indicating that this mutation has multiple effects of the gating of these channels (Sanchez et al., 2014).

Although not a KIDS mutation, M151L has been reported to be associated with deafness (Siemering et al., 2006). Our finding that it prevents functional gap junction communication suggests possible underlying mechanistic cause of hearing loss with this mutation. The endocochlear potential is essential for hearing -it provides the driving force for K^+ to enter the hair cells through the mechanosensory ion channels present in their stereocillia. Cx26 gap junctions are a pathway for diffusion of K^+ between the fibrocytes, basal cells and intermediate cells of the stria vascularis (Wangemann, 2006) and have been proposed to form part of the pathway that recycles K^+ away from the hair cells and back into the endolymph, although this has been disputed (Zhao, 2017). Genetic deletion of Cx26 reduces the endocochlear potential by about half (Chen et al., 2014). Given that M151L prevents gap junction coupling (although not the formation of gap junctions *per se*), we predict that it would reduce the endocochlear potential and that this is the reason for hearing impairment.

Physiological implications

As Cx26 exists both as gap junctions and hemichannels, our findings have substantial physiological significance. In the context of breathing, Cx26 hemichannels are important and we have already explored their significance for chemosensory control (Huckstepp et al., 2010b). However, there are reports of gap junctions in various nuclei implicated in the control of breathing (Dean et al., 2002; Solomon et al., 2003). CO_2-dependent uncoupling of Cx26 gap junctions between cells may therefore be an additional mechanism that contributes to chemosensory control.

In lungfish and amphibia, hemichannels of Cx26 are insensitive to CO_2 despite possessing the carbamylation motif (Dospinescu et al., 2019). The extended C-terminal tail of Cx26 in these species interferes with hemichannel opening. However, the Cx26 gap junctions of these species can still be closed by CO_2 (Dospinescu et al., 2019). The ancestral function of the carbamylation motif in Cx26 was therefore most likely to close the gap junction and the new function of hemichannel opening only arose in the amniotes (Dospinescu et al., 2019). Given that it has been conserved over many hundreds of millions of years, the CO_2-dependent closure of Cx26 gap junctions must have some important physiological function. What this may be remains open to question, but we speculate that if a single cell in a coupled network were to be excessively metabolically active, it would act as a sink for metabolites such as ATP, glucose or lactate from the coupled cells. As the metabolically active cell would produce more CO_2 this could be a self-regulating mechanism to preserve network

integrity by uncoupling the "run-away" cell from the network thereby reducing its drain on the communal pool of metabolites. It is interesting in this context, that the PCO_2 of renal cortex and liver (respectively 57 and 64 mmHg), two organs where Cx26 and Cx32 are abundantly expressed, is considerably higher than the PCO_2 of systemic circulation (39-45 mmHg) (Hogg et al., 1984).

Methods

HeLa cell culture and transfection

HeLa DH (ECACC) cells were grown in DMEM supplemented with 10% fetal bovine serum, 50 µg/mL penicillin/streptomycin and 3 mM $CaCl_2$. For electrophysiology and intercellular dye transfer experiments, cells were seeded onto coverslips in 6 well plates at a density of $2x10^4$ cells per well. After 24hrs the cells were transiently transfected with Cx26 constructs tagged at the C-terminus with a fluorescent marker (mCherry) according to the GeneJuice Transfection Reagent protocol (Merck Millipore).

Solutions used

Standard aCSF: 124 mM NaCl, 3 mM KCl, 2 mM $CaCl_2$, 26 mM $NaHCO_3$, 1.25 mM NaH_2PO_4, 1 mM $MgSO_4$, 10 mM D-glucose saturated with 95% O_2/5% CO_2, pH 7.5, PCO_2 35 mmHg.

Hypercapnic aCSF: 100 mM NaCl, 3 mM KCl, 2 mM $CaCl_2$, 50 mM $NaHCO_3$, 1.25 mM NaH_2PO_4, 1 mM $MgSO_4$, 10 mM D-glucose, saturated with 9% CO_2 (with the balance being O_2) to give a pH of 7.5 and a PCO_2 of 55 mmHg respectively.

Propionate solution: 82mM NaCl, 30 mM Na-propionate, 3 mM KCl, 2 mM $CaCl_2$, 26 mM $NaHCO_3$, 1.25 mM NaH_2PO_4, 1 mM $MgSO_4$, 10 mM D-glucose saturated with 95% O_2/5% CO_2, pH 7.5, PCO_2 35 mmHg.

Patch Clamp recordings

Cover slips containing non-confluent cells were placed into a perfusion chamber at room temperature in sterile filtered standard aCSF. Standard patch clamp techniques were used to make whole-cell recordings from either single HeLa cells or pairs of HeLa cells. The intracellular fluid in the patch pipettes contained: K-gluconate 120 mM, CsCl 10 mM, TEACl 10 mM, EGTA 10 mM, ATP 3 mM, $MgCl_2$ 1 mM, $CaCl_2$ 1 mM, sterile filtered, pH adjusted to 7.2 with KOH. All whole-cell recordings were performed at a holding potential of -50 mV with regular steps of 5 s to -50 mV to assess whole-cell conductance.

Cx26 mutants

The mutations used in this study were introduced into the Cx26 gene by QuikChange site directed mutagenesis and have been described previously (Meigh et al., 2013) (Cook et al., 2019).

Imaging assay of gap junction transfer

2-Deoxy-2-[(7-nitro-2,1,3-benzoxadiazol-4-yl)amino]-D-glucose, NBDG, was included at 200 μM in the patch recording fluid which was either the same as above or had lowered EGTA concentration (5mM). Cells were imaged on a Cleverscope (MCI Neuroscience) with a Photometrics Prime camera under the control of Micromanager 1.4 software. LED illumination (Cairn Research) and an image splitter (Optosplit, Cairn Research) allowed simultaneous imaging of the mCherry tagged Cx26 subunits and the diffusion of the NBDG into and between cells. Cells were selected for patch clamp recordings on the basis of their expression of mCherry-tagged Cx26 protein and the presence of gap junction plaques formed between the two cells, which were easily visible as a band of mCherry fluorescence (e.g. Figures 5 and 9). Following breakthrough of the patch pipette to establish the whole cell mode, images were collected every 10 seconds.

Elastic network modelling

Elastic network model (ENM) simulations were performed based on the regular implementation using PDB file 2ZW3, where all the Cα atoms in the protein within a given cut-off radius (8 Å) were joined with simple Hookean springs (Rodgers et al., 2013a; Tirion, 1996). The spring constants were set to a constant value of 1 kcal mol^{-1} $Å^{-2}$. The presence of CO_2 was represented in the ENM by the inclusion of an additional Hookean spring between residues K125 and R104 of each set of neighbouring monomers, following the same procedure previously used for ligand binding (Rodgers et al., 2013b). The mass-weighted second derivatives of this potential energy matrix were diagonalised to produce eigenvectors, e, which are the normal modes, and eigenvalues which are the squares of the associated frequencies, ω, and can be used to calculate the free energy of each mode.

The first six modes, that is the lowest frequency modes, represent the solid body translational and rotational motions of the protein and are thus ignored from the analysis. The overlap of the modes in the unbound and CO_2 bound states were calculated by comparison of the eigenvectors (Rodgers et al., 2013a). A value of 1 indicates that the motions are identical whereas a value of 0 indicates that the motions are completely different.

Statistics and Reproducibiity

Statistical analysis was performed with the R language. Data has been plotted as box and whisker plots, with individual points superimposed, where the box is interquartile range, bar is median, and whisker extends to most extreme data point that is no more than 1.5 times the interquartile range. Each individual point is from a single patch clamp experiment and is counted as a replicate. Statistical comparisons were performed with the Krusak Wallis test (for multiple comparisons) or Mann Whiney U test. Exact p values are shown for comparisons that showed a significant difference between samples.

Acknowledgements

We thank the MRC (MR/P010393/1) for support. ND is a Royal Society Wolfson Research Merit Award Holder.

Author contributions

DM, SN, ND: Patch clamping, data collection and analysis

LM, EdW: Generation of mutants and stable cell lines

TR, MC: Elastic network modelling

ND wrote the paper, all authors commented on the final version.

Conflict of Interest Statement

The authors declare that they have no conflicts of interest.

Data availability

All data generated or analysed during this study are included in this published article (and its supplementary information files) or are available from the authors upon reasonable request.

References

Chen, J., Chen, J., Zhu, Y., Liang, C., and Zhao, H.B. (2014). Deafness induced by Connexin 26 (GJB2) deficiency is not determined by endocochlear potential (EP) reduction but is associated with cochlear developmental disorders. Biochem Biophys Res Commun *448*, 28-32.

Cook, J., de Wolf, E., and Dale, N. (2019). Cx26 keratitis ichthyosis deafness syndrome mutations trigger alternative splicing of Cx26 to prevent expression and cause toxicity in vitro. Royal Society open science *6*, 191128.

De Vuyst, E., Decrock, E., De Bock, M., Yamasaki, H., Naus, C.C., Evans, W.H., and Leybaert, L. (2007). Connexin hemichannels and gap junction channels are differentially influenced by lipopolysaccharide and basic fibroblast growth factor. Mol Biol Cell *18*, 34-46.

de Wolf, E., Cook, J., and Dale, N. (2017). Evolutionary adaptation of the sensitivity of connexin26 hemichannels to CO2. Proc R Soc B *284: 20162723*.

de Wolf, E., van de Wiel, J., Cook, J., and Dale, N. (2016). Altered CO2 sensitivity of connexin26 mutant hemichannels in vitro. Physiol Rep *4*, e13038.

Dean, J.B., Ballantyne, D., Cardone, D.L., Erlichman, J.S., and Solomon, I.C. (2002). Role of gap junctions in CO(2) chemoreception and respiratory control. Am J Physiol Lung Cell Mol Physiol *283*, L665-670.

Delarue, M., and Sanejouand, Y.H. (2002). Simplified normal mode analysis of conformational transitions in DNA-dependent polymerases: the elastic network model. J Mol Biol *320*, 1011-1024.
Dospinescu, V.-M., Nijjar, S., Spanos, F., Cook, J., de Wolf, E., Biscotti, M.A., Gerdol, M., and Dale, N. (2019). Structural determinants of CO2-sensitivity in the β connexin family suggested by evolutionary analysis. Communications Biology *2*, 331.
Haussig, S., Schubert, A., Mohr, F.W., and Dhein, S. (2008). Sub-chronic nicotine exposure induces intercellular communication failure and differential down-regulation of connexins in cultured human endothelial cells. Atherosclerosis *196*, 210-218.
Hogg, R.J., Pucacco, L.R., Carter, N.W., Laptook, A.R., and Kokko, J.P. (1984). In situ PCO2 in the renal cortex, liver, muscle, and brain of the New Zealand white rabbit. Am J Physiol *247*, F491-498.
Huckstepp, R.T., and Dale, N. (2011). Redefining the components of central CO2 chemosensitivity--towards a better understanding of mechanism. J Physiol *589*, 5561-5579.
Huckstepp, R.T., Eason, R., Sachdev, A., and Dale, N. (2010a). CO2-dependent opening of connexin 26 and related beta connexins. J Physiol *588*, 3921-3931.
Huckstepp, R.T., id Bihi, R., Eason, R., Spyer, K.M., Dicke, N., Willecke, K., Marina, N., Gourine, A.V., and Dale, N. (2010b). Connexin hemichannel-mediated CO2-dependent release of ATP in the medulla oblongata contributes to central respiratory chemosensitivity. J Physiol *588*, 3901-3920.
Isin, B., Tirupula, K.C., Oltvai, Z.N., Klein-Seetharaman, J., and Bahar, I. (2012). Identification of motions in membrane proteins by elastic network models and their experimental validation. Methods Mol Biol *914*, 285-317.
Jahromi, S.S., Wentlandt, K., Piran, S., and Carlen, P.L. (2002). Anticonvulsant actions of gap junctional blockers in an in vitro seizure model. J Neurophysiol *88*, 1893-1902.
Kang, J., Kang, N., Lovatt, D., Torres, A., Zhao, Z., Lin, J., and Nedergaard, M. (2008). Connexin 43 hemichannels are permeable to ATP. J Neurosci *28*, 4702-4711.
Lopez, W., Gonzalez, J., Liu, Y., Harris, A.L., and Contreras, J.E. (2013). Insights on the mechanisms of Ca(2+) regulation of connexin26 hemichannels revealed by human pathogenic mutations (D50N/Y). J Gen Physiol *142*, 23-35.
Lorimer, G.H. (1983). Carbon-Dioxide and Carbamate Formation - the Makings of a Biochemical Control-System. Trends in Biochemical Sciences *8*, 65-68.
Maeda, S., Nakagawa, S., Suga, M., Yamashita, E., Oshima, A., Fujiyoshi, Y., and Tsukihara, T. (2009). Structure of the connexin 26 gap junction channel at 3.5 A resolution. Nature *458*, 597-602.
Meigh, L., Cook, D., Zhang, J., and Dale, N. (2015). Rational design of new NO and redox sensitivity into connexin26 hemichannels. Open Biol *5*, 140208.
Meigh, L., Greenhalgh, S.A., Rodgers, T.L., Cann, M.J., Roper, D.I., and Dale, N. (2013). CO2 directly modulates connexin 26 by formation of carbamate bridges between subunits. eLife *2*, e01213.
Meigh, L., Hussain, N., Mulkey, D.K., and Dale, N. (2014). Connexin26 hemichannels with a mutation that causes KID syndrome in humans lack sensitivity to CO2. eLife *3*, e04249.
Mese, G., Sellitto, C., Li, L., Wang, H.Z., Valiunas, V., Richard, G., Brink, P.R., and White, T.W. (2011). The Cx26-G45E mutation displays increased hemichannel activity in a mouse model of the lethal form of keratitis-ichthyosis-deafness syndrome. Mol Biol Cell *22*, 4776-4786.
Montgomery, J.R., White, T.W., Martin, B.L., Turner, M.L., and Holland, S.M. (2004). A novel connexin 26 gene mutation associated with features of the keratitis-ichthyosis-deafness syndrome and the follicular occlusion triad. Journal of the American Academy of Dermatology *51*, 377-382.
Pearson, R.A., Dale, N., Llaudet, E., and Mobbs, P. (2005). ATP released via gap junction hemichannels from the pigment epithelium regulates neural retinal progenitor proliferation. Neuron *46*, 731-744.
Retamal, M.A., Froger, N., Palacios-Prado, N., Ezan, P., Sáez, P.J., Sáez, J.C., and Giaume, C. (2007a). Cx43 Hemichannels and Gap Junction Channels in Astrocytes Are Regulated Oppositely by Proinflammatory Cytokines Released from Activated Microglia. The Journal of Neuroscience *27*, 13781-13792.

Retamal, M.A., Schalper, K.A., Shoji, K.F., Bennett, M.V., and Saez, J.C. (2007b). Opening of connexin 43 hemichannels is increased by lowering intracellular redox potential. Proc Natl Acad Sci U S A *104*, 8322-8327.
Rodgers, T.L., Burnell, D., Townsend, P.D., Pohl, E., Cann, M.J., Wilson, M.R., and McLeish, T.C. (2013a). ΔΔPT: a comprehensive toolbox for the analysis of protein motion. BMC Bioinformatics *14*, 183.
Rodgers, T.L., Townsend, P.D., Burnell, D., Jones, M.L., Richards, S.A., McLeish, T.C., Pohl, E., Wilson, M.R., and Cann, M.J. (2013b). Modulation of Global Low-Frequency Motions Underlies Allosteric Regulation: Demonstration in CRP/FNR Family Transcription Factors. PLoS Biol *11*, e1001651.
Sanchez, H.A., Bienkowski, R., Slavi, N., Srinivas, M., and Verselis, V.K. (2014). Altered Inhibition of Cx26 Hemichannels by pH and Zn2+ in the A40V Mutation Associated with Keratitis-Ichthyosis-Deafness Syndrome. J Biol Chem *289*, 21519-21532.
Sanchez, H.A., Mese, G., Srinivas, M., White, T.W., and Verselis, V.K. (2010). Differentially altered Ca2+ regulation and Ca2+ permeability in Cx26 hemichannels formed by the A40V and G45E mutations that cause keratitis ichthyosis deafness syndrome. J Gen Physiol *136*, 47-62.
Sanchez, H.A., Slavi, N., Srinivas, M., and Verselis, V.K. (2016). Syndromic deafness mutations at Asn 14 differentially alter the open stability of Cx26 hemichannels. J Gen Physiol *148*, 25-42.
Sherwood, P., Brooks, B.R., and Sansom, M.S. (2008). Multiscale methods for macromolecular simulations. Current opinion in structural biology *18*, 630-640.
Shrivastava, I.H., and Bahar, I. (2006). Common mechanism of pore opening shared by five different potassium channels. Biophys J *90*, 3929-3940.
Siemering, K., Manji, S.S., Hutchison, W.M., Du Sart, D., Phelan, D., and Dahl, H.H. (2006). Detection of mutations in genes associated with hearing loss using a microarray-based approach. J Mol Diagn *8*, 483-489; quiz 528.
Solomon, I.C., Chon, K.H., and Rodriguez, M.N. (2003). Blockade of brain stem gap junctions increases phrenic burst frequency and reduces phrenic burst synchronisation in adult rat. Journal of neurophysiology *89*, 135-149.
Stout, C., Goodenough, D.A., and Paul, D.L. (2004). Connexins: functions without junctions. Curr Opin Cell Biol *16*, 507-512.
Stout, C.E., Costantin, J.L., Naus, C.C., and Charles, A.C. (2002). Intercellular calcium signaling in astrocytes via ATP release through connexin hemichannels. J Biol Chem *277*, 10482-10488.
Tirion, M.M. (1996). Large Amplitude Elastic Motions in Proteins from a Single-Parameter, Atomic Analysis. Physical review letters *77*, 1905-1908.
Valadie, H., Lacapcre, J.J., Sanejouand, Y.H., and Etchebest, C. (2003). Dynamical properties of the MscL of Escherichia coli: a normal mode analysis. J Mol Biol *332*, 657-674.
Valdez Capuccino, J.M., Chatterjee, P., Garcia, I.E., Botello-Smith, W.M., Zhang, H., Harris, A.L., Luo, Y., and Contreras, J.E. (2019). The connexin26 human mutation N14K disrupts cytosolic intersubunit interactions and promotes channel opening. J Gen Physiol *151*, 328-341.
Wangemann, P. (2006). Supporting sensory transduction: cochlear fluid homeostasis and the endocochlear potential. J Physiol *576*, 11-21.
Weissman, T.A., Riquelme, P.A., Ivic, L., Flint, A.C., and Kriegstein, A.R. (2004). Calcium waves propagate through radial glial cells and modulate proliferation in the developing neocortex. Neuron *43*, 647-661.
Young, K.C., and Peracchia, C. (2004). Opposite Cx32 and Cx26 voltage-gating response to CO2 reflects opposite voltage-gating polarity. J Membr Biol *202*, 161-170.
Yu, J., Bippes, C.A., Hand, G.M., Muller, D.J., and Sosinsky, G.E. (2007). Aminosulfonate modulated pH-induced conformational changes in connexin26 hemichannels. J Biol Chem *282*, 8895-8904.
Zhang, Y., and Hao, H. (2013). Conserved glycine at position 45 of major cochlear connexins constitutes a vital component of the Ca(2)(+) sensor for gating of gap junction hemichannels. Biochem Biophys Res Commun *436*, 424-429.
Zhao, H.B. (2017). Hypothesis of K(+)-Recycling Defect Is Not a Primary Deafness Mechanism for Cx26 (GJB2) Deficiency. Frontiers in molecular neuroscience *10*, 162.

Zheng, W., and Auerbach, A. (2011). Decrypting the Sequence of Structural Events during the Gating Transition of Pentameric Ligand-Gated Ion Channels Based on an Interpolated Elastic Network Model. PLOS Computational Biology *7*, e1001046.

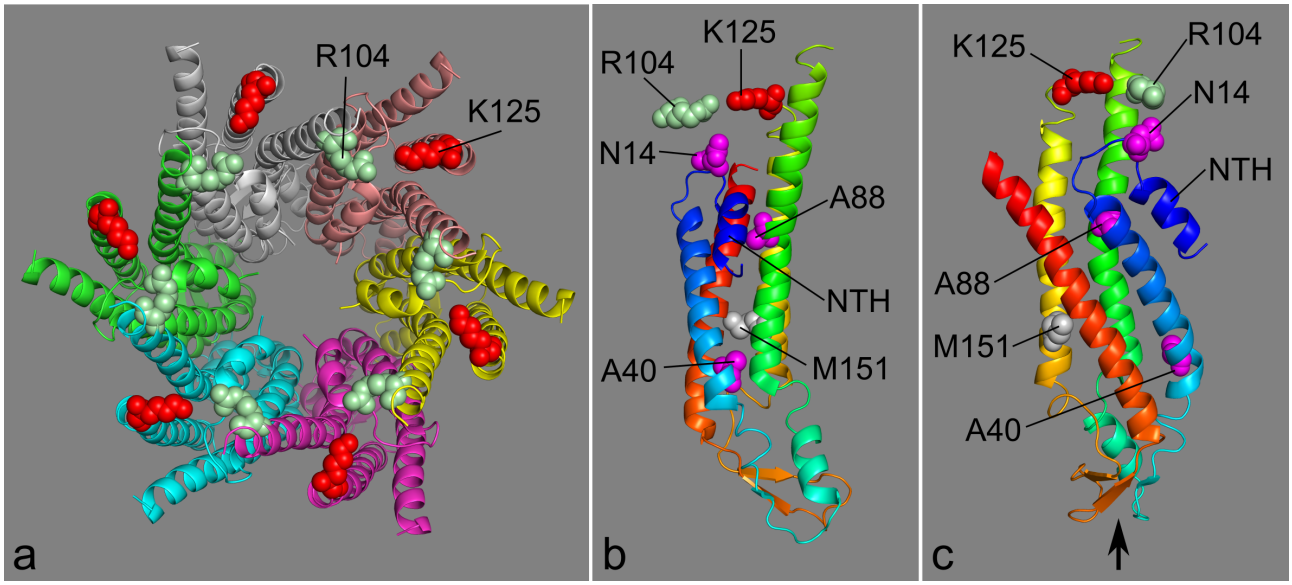

Figure 1. Position of the Cx26 carbamylation motif relative to the residues mutated in this study. a) View of the hemichannel as seen from the cytoplasmic face. Residues K125 and R104 of the carbamylation motif are shown in red and light green respectively. b) Side view of a single subunit showing the positions of mutated residues (N14, A40 and A88 are mutated in KIDS, M151 was mutated to prevent alternative splicing of KIDS mutated mRNA). R104 from the adjacent subunit is shown aligned to K125 of the subunit. NTH: N terminal helix. c) Additional view of the subunit after rotating it approximately 90^0 counterclockwise. Arrow indicates the loops in the subunit that dock to a hexamer in an opposed membrane to form a gap junction. Structure based on 2zw3 from the Protein Database.

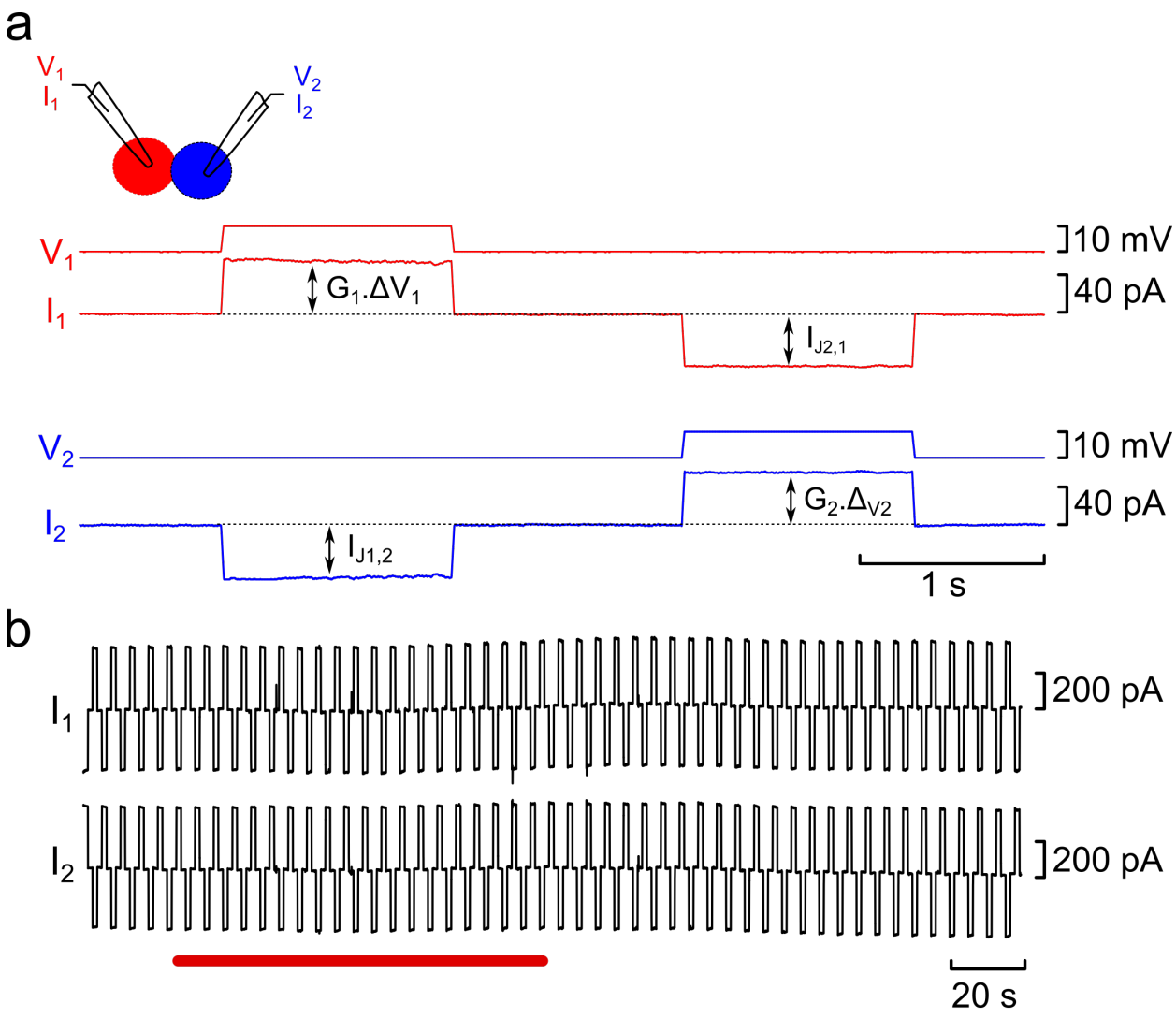

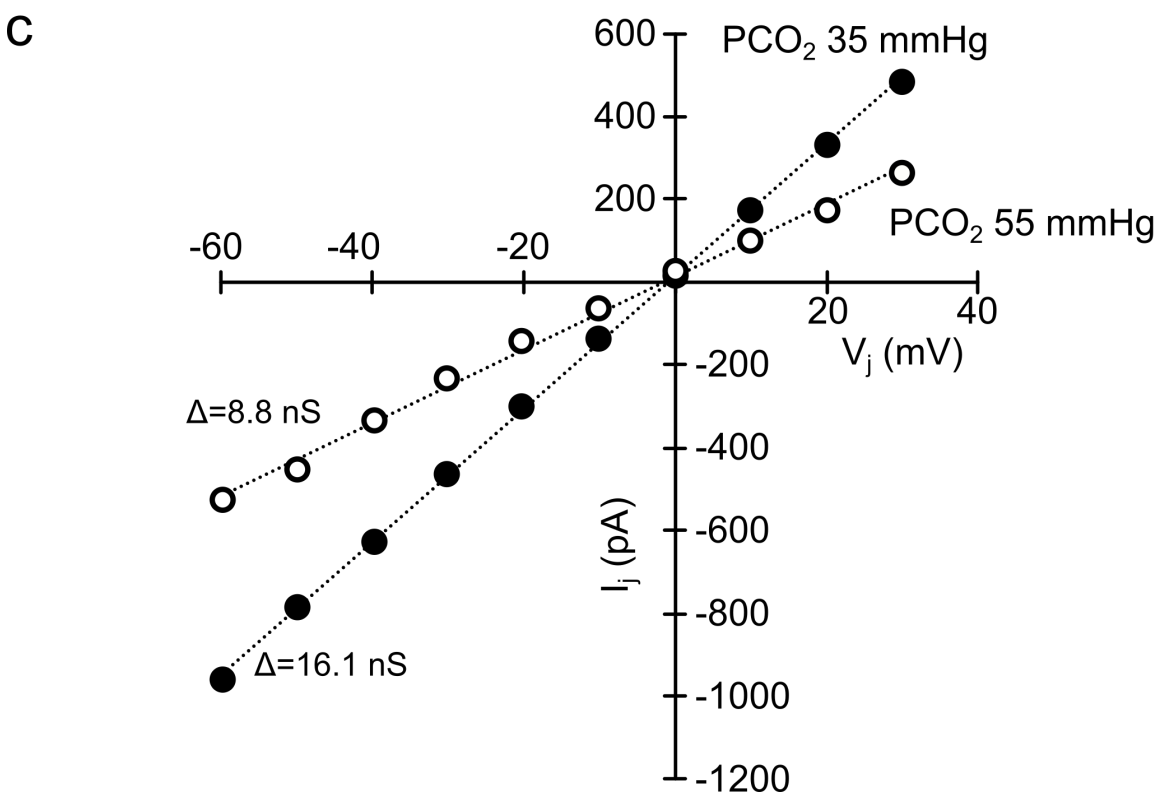

Figure 2. Voltage clamp protocol to measure simultaneously the whole cell conductance and junctional conductance in pairs of coupled HeLa cells. a) Both cells are clamped at -50 mV, and subjected to alternating 10 mV steps. $I_{J1,2}$ –current flow from cell 1 to cell 2; $I_{J2,1}$ –current flow from cell 2 to cell 1; G_1 –whole cell conductance of cell 1; G_2 –whole cell conductance of cell 2. Opening of Cx26 hemichannels will increase the whole cell conductance, whereas closure of Cx26 gap junctions will decrease $I_{J1,2}$ and $I_{J2,1}$ and decrease the whole cell conductance. The junctional conductance is simply $I_{J1,2}/(V_1-V_2)$ or $I_{J2,1}/(V_2-V_1)$. As Cx26 gap junctions display no rectification, both methods give the same value. b) Parental HeLa cells (not transfected with Cx26) can display gap junction coupling but this was insensitive to CO_2 (red bar represents application of hypercapnic saline). c) Cx26 gap junctions in transfected HeLa cells display a linear current-voltage relation (2 s voltage steps, from -80 to +10 mV, while second cell clamped at -50 mV). Dotted line, best fitting regression line, the gap junction conductance (Δ) was approximately halved by raised PCO_2 (open circles) at all transjunctional voltages. V_j transjunctional voltage, I_j gap junction current.

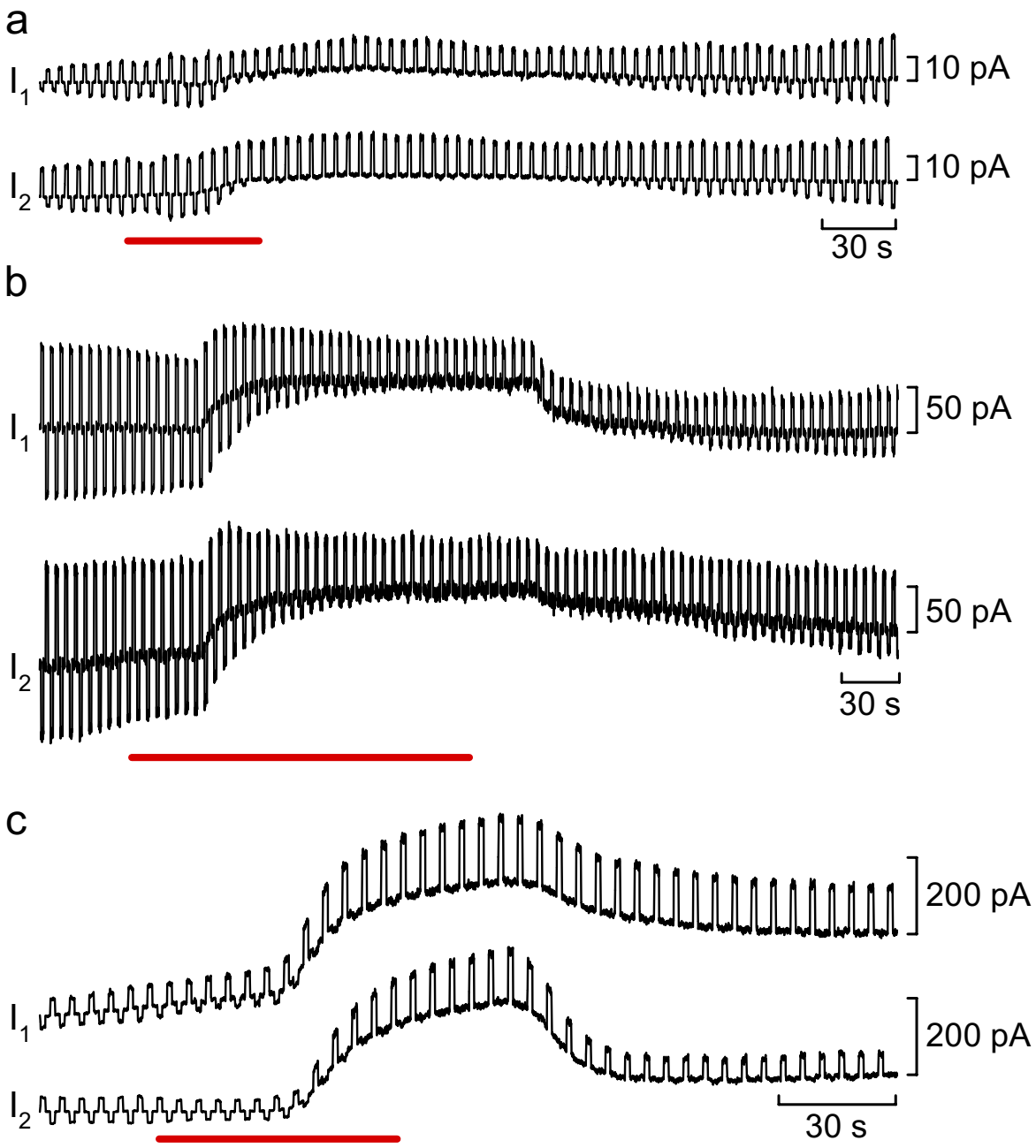

Figure 3. CO_2 closes Cx26 gap junctions. a) Hypercapnic saline (PCO_2 55 mmHg) applied at red bar, caused complete and reversible closure of the gap junction. In this instance the junctional conductance and hemichannel conductances were roughly equal hence, there was little overall net change in whole cell conductance (compare to model currents in Figure 4a). b) In a different pair of cells, hypercapnic saline (red bar) caused complete and reversible gap junction closure. Overall there was a reduction in the whole cell conductance -as a result of gap junction closure. This example is comparable to the case where the gap junction conductance exceeds that of the hemichannels in the cells (compare to model currents in Figure 4b). c) In this example the gap junction closure during hypercapnia (red bar) was complete and did not reverse during the recording, although hemichannel

opening did reverse. This example is comparable to the model currents in Figure 4c where the hemichannel conductance exceeds that of the gap junction conductance. The delay between the onset of gap junction modulation and application of hypercapnic saline results from the characteristics of the bath flow system.

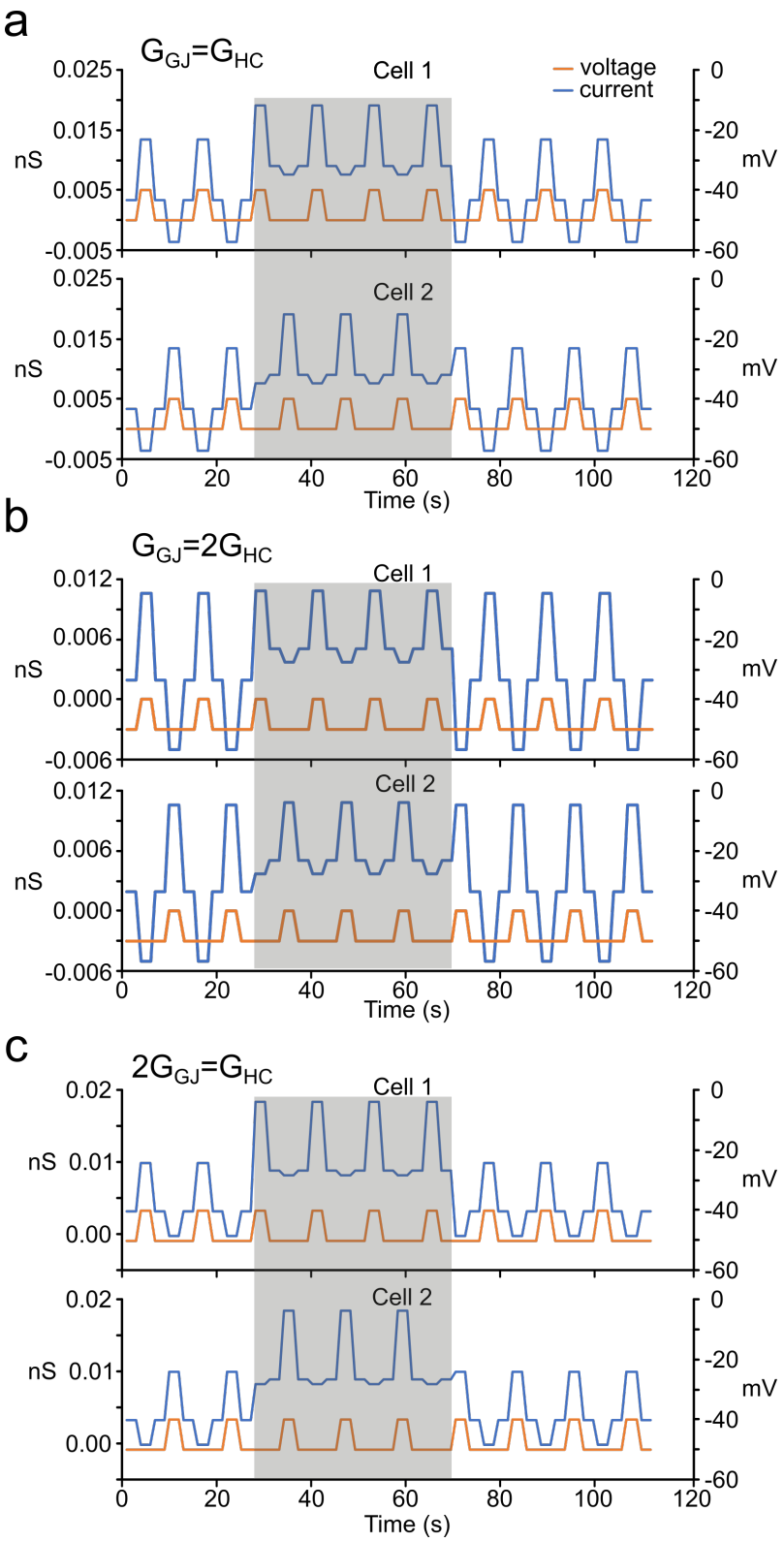

Figure 4. Calculation of model whole cell currents before and during CO_2 application. This very simple model is designed to assist the interpretation of whole cell recordings where there are variable proportions of hemichannels and gap junctions that are simultaneously and oppositely modulated by CO_2. a) Calculated currents where the hemichannel conductance in each cell equals

the gap junction conductance between cells. b) In this case the gap junction conductance is twice that of the hemichannel conductance (same in each cell). c) This is an example of the opposite case where the hemichannel conductance in each cell is twice that of the gap junction conductance. The grey box indicates the period of elevated PCO_2 (55 mmHg).

The model, available in an Excel spreadsheet, comprised of 2 coupled cells each having three currents:

$$I=f.I_{HC}+I_L+(1-f).I_{GJ}$$

where *f* has a value between 0 and 1 and is a function of PCO_2.

For cell 1 these currents would be:

$$I_{HC}=g_{HC}(V-V_{rev});\ I_L=g_L(V-V_L);\ I_{GJ}=g_{GJ}(V_1-V_2)$$

Where I_{HC} is the hemichannel current; I_{GJ} the gap junction current; and I_L the leak current. g_{HC} is the hemichannel conductance; g_{GJ} the gap junction conductance; and g_L the leak conductance.
V_{rev} was set empirically to -61mV (apparent reversal potential for Cx26 under these ionic conditions); V_L was set to -70 mV to represent a generic leak current largely K^+ driven. V_1 is the membrane potential of cell 1 and V_2 the membrane potential of cell 2. The equations for cell 2 would be equivalent.

A very simple model for CO_2 modulation of the hemichannel and gap junction based on the Hill equation was used:

$$f=(PCO_2/K)^H/[1+(PCO_2/K)^H].$$

K was set to 40 mmHg, and *H* to 6, values based on previously published data (Huckstepp et al., 2010a).

For simplicity, modulation of the gap junction by CO_2 was *1-f*.

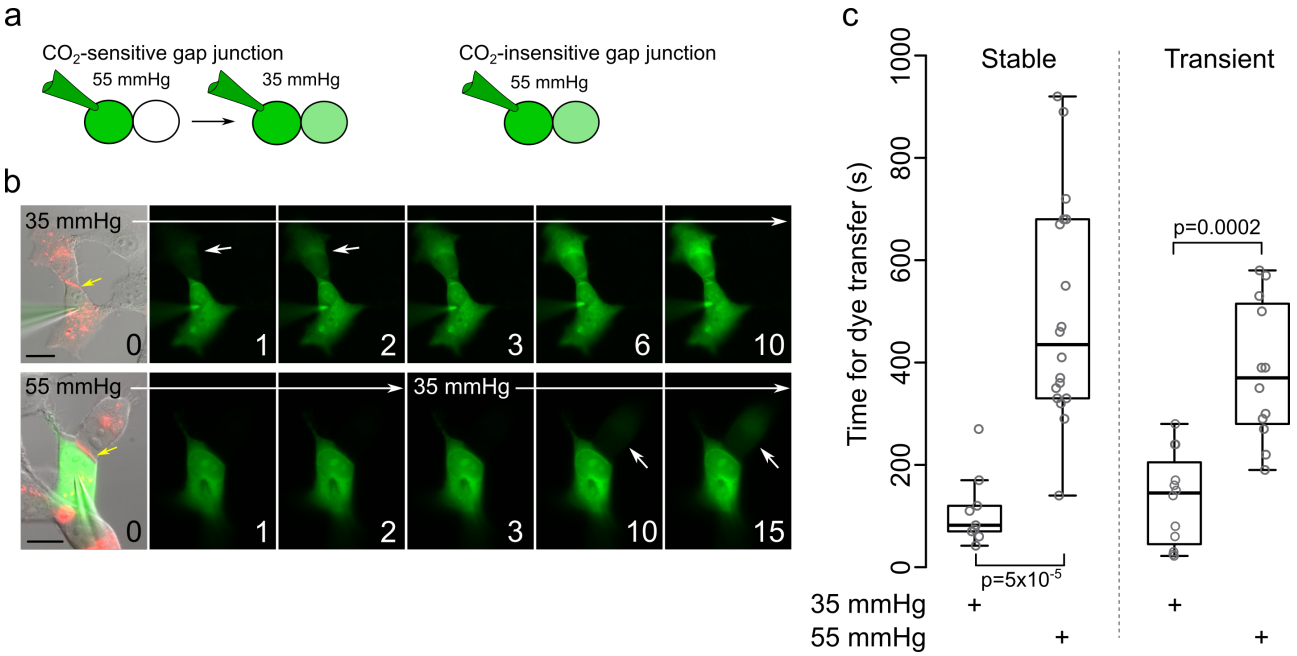

Figure 5. Dye transfer assay to assess the CO_2 sensitivity of gap junction coupling. a) Logic of the assay: a CO_2 sensitive gap junction will display no or very little dye transfer from the donor to acceptor cell under conditions of high PCO_2. This will occur once the cells are transferred to a low PCO_2 saline. A CO_2 insensitive gap junction will exhibit equally rapid dye transfer at low and high PCO_2. b) Images showing dye transfer between coupled cells at two different levels of PCO_2. Numbers in lower right corner are recording time in minutes. Picture at 0 minutes in both rows is a merge of DIC and mCherry (for Cx26, red) and NBDG fluorescence (green) and is the beginning of the recording. The gap junction can be observed as a red stripe between the coupled cells (yellow arrows, both rows). Subsequent pictures show just the NBDG fluorescence. In 35 mmHg PCO_2 dye transfer to the acceptor cell is evident after 1 minute (white arrows). Starting the recording at a PCO_2 of 55 mmHg, and then transferring to 35 mmHg saline after 2 minutes greatly slows dye transfer; fluorescence in the acceptor cell is only seen after 10 minutes (white arrows). Scale bar is 20 μm. c) Summary data for stably expressing (n=9 and 18 for low and high CO_2 respectively) and transiently transfected (n=12 for low and high CO_2) HeLa cells, showing the time for dye in the acceptor cell to reach 10% of the donor starting in 35 mmHg, and starting in 55 mmHg but transferring to 35mmHg after two minutes. When the recordings are commenced in 55 mmHg the dyes transfer time is much longer. Statistical comparisons Mann Whitney U test.

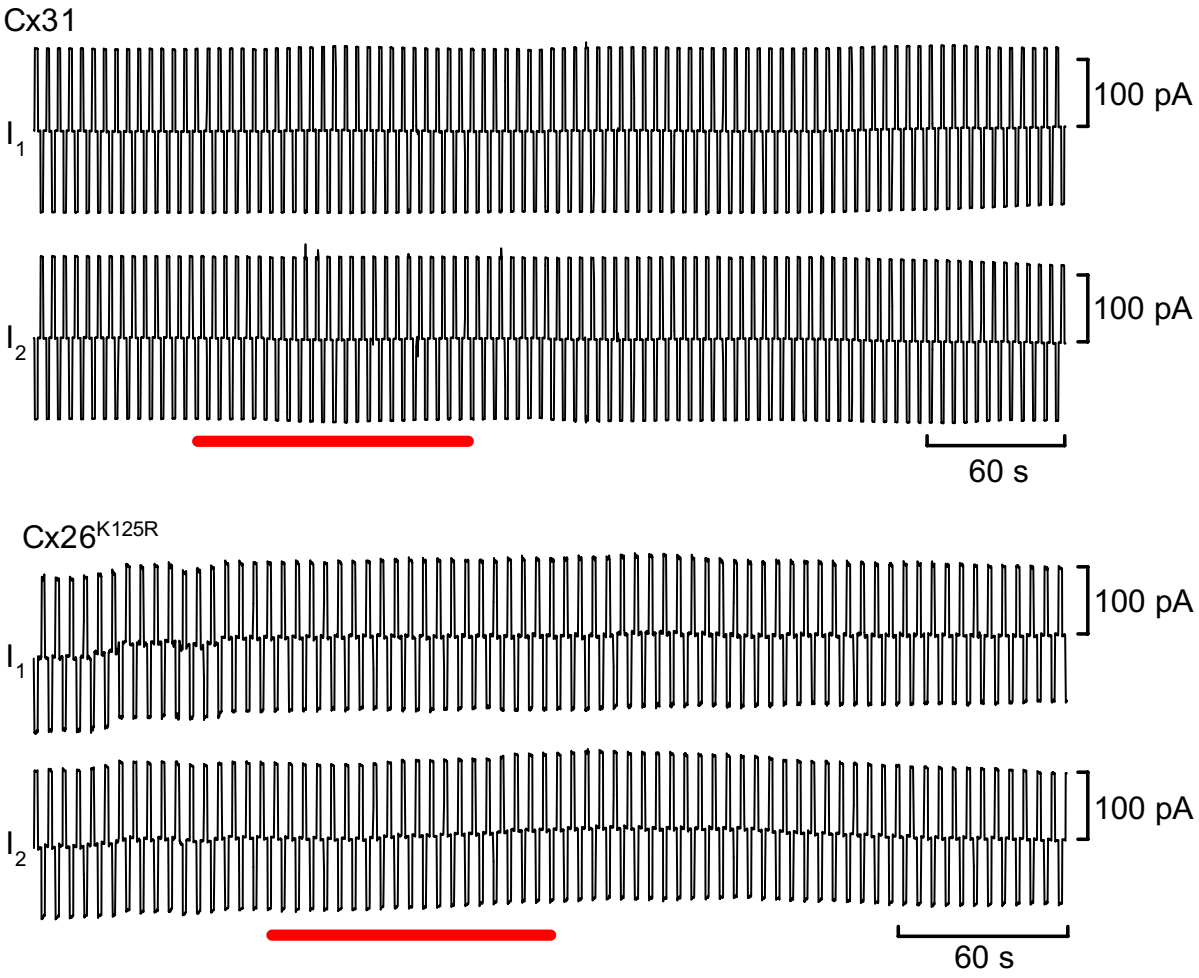

Figure 6. The CO_2 dependence of Cx26 gap junctions requires the carbamylation motif. Top) Cx31 gap junctions, which lack the carbamylation motif, are insensitive to CO_2. The mutation K125R which removes CO_2 sensitivity from the hemichannel also removes CO_2 sensitivity of the gap junction. Experiments performed on HeLa cells stably transfected with the Cx31 or $Cx26^{K125R}$. Red bar represents application of hypercapnic saline.

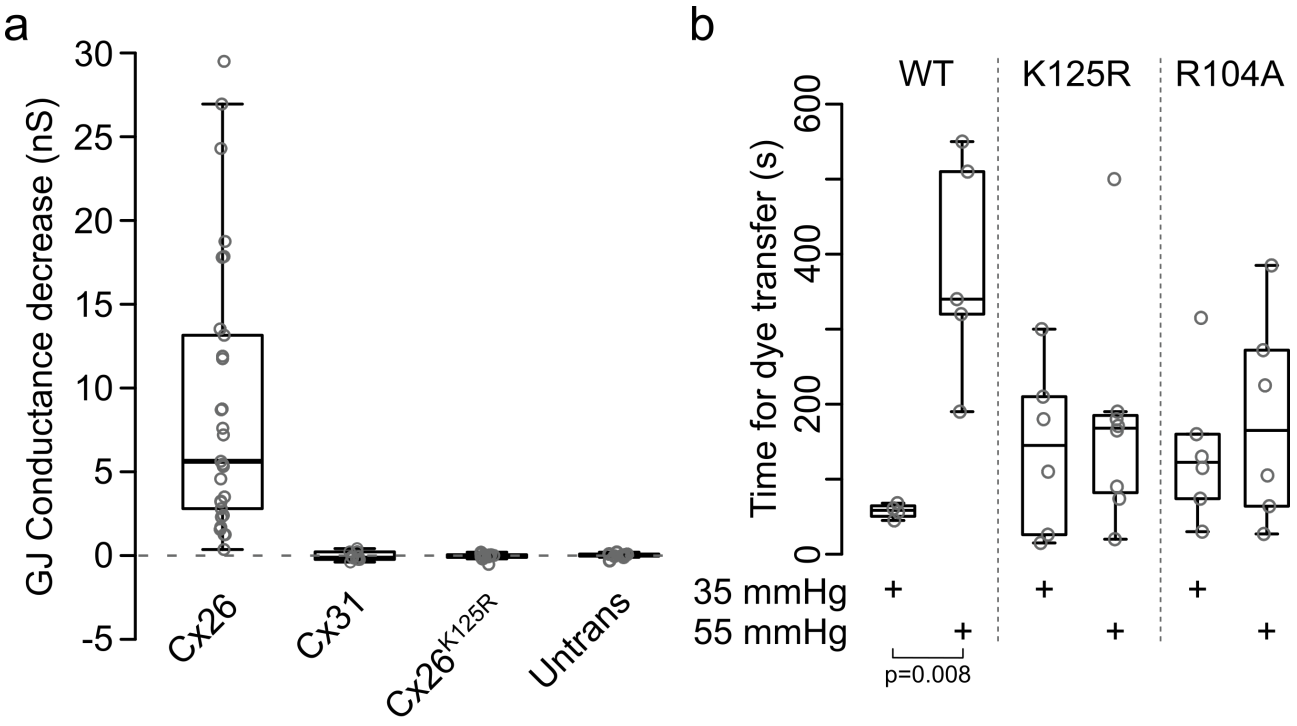

Figure 7. CO_2 dependence of Cx26 gap junction closing depends on the carbamylation motif. a) Gap junctions in HeLa cells Cx31 and $Cx26^{K125R}$ exhibit no CO_2-dependence. Gap junctions occasionally seen between parental HeLa cells (Untrans) display no CO_2-dependence either. Only WT Cx26 gap junctions exhibit a CO_2-dependent conductance decrease. b) Dye transfer assays show that WT Cx26 gap junctions are clearly CO_2 sensitive (55 mmHg PCO_2 delays the passage of dye across the gap junction), but those comprised of $Cx26^{K125R}$ or $Cx26^{R104A}$ show no CO_2-dependence in the time required for dye transfer from the donor to acceptor cell. Mann Whitney U test WT 35mmHg vs WT 55 mmHg, p=0.008.

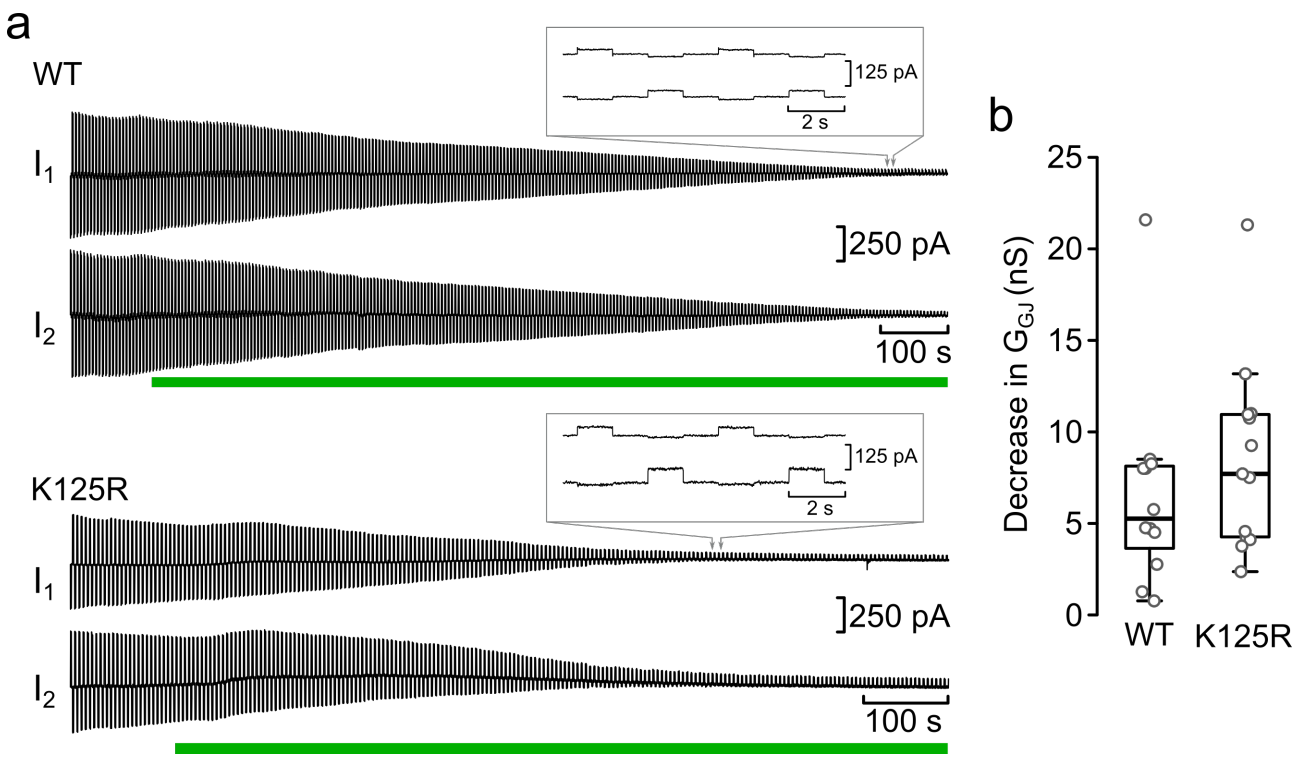

Figure 8. Intracellular acidification closes Cx26 gap junctions and is independent of the carbamylation motif. a) Sample recordings of gap junctions formed between cells transiently expressing $Cx26^{WT}$ or $Cx26^{K125R}$. The same voltage protocol as Figure 2a was used to measure the gap junction current. Application of 30 mM propionate (green bar) caused a reduction in the gap junction currents, that was similar for $Cx26^{WT}$ and $Cx26^{K125R}$. The insets show the current traces at indicated time when Gap junction blockade was almost complete. b) Summary data showing the gap junction conductance decrease caused by acidification of HeLa cells expressing $Cx26^{WT}$ or $Cx26^{K125R}$.

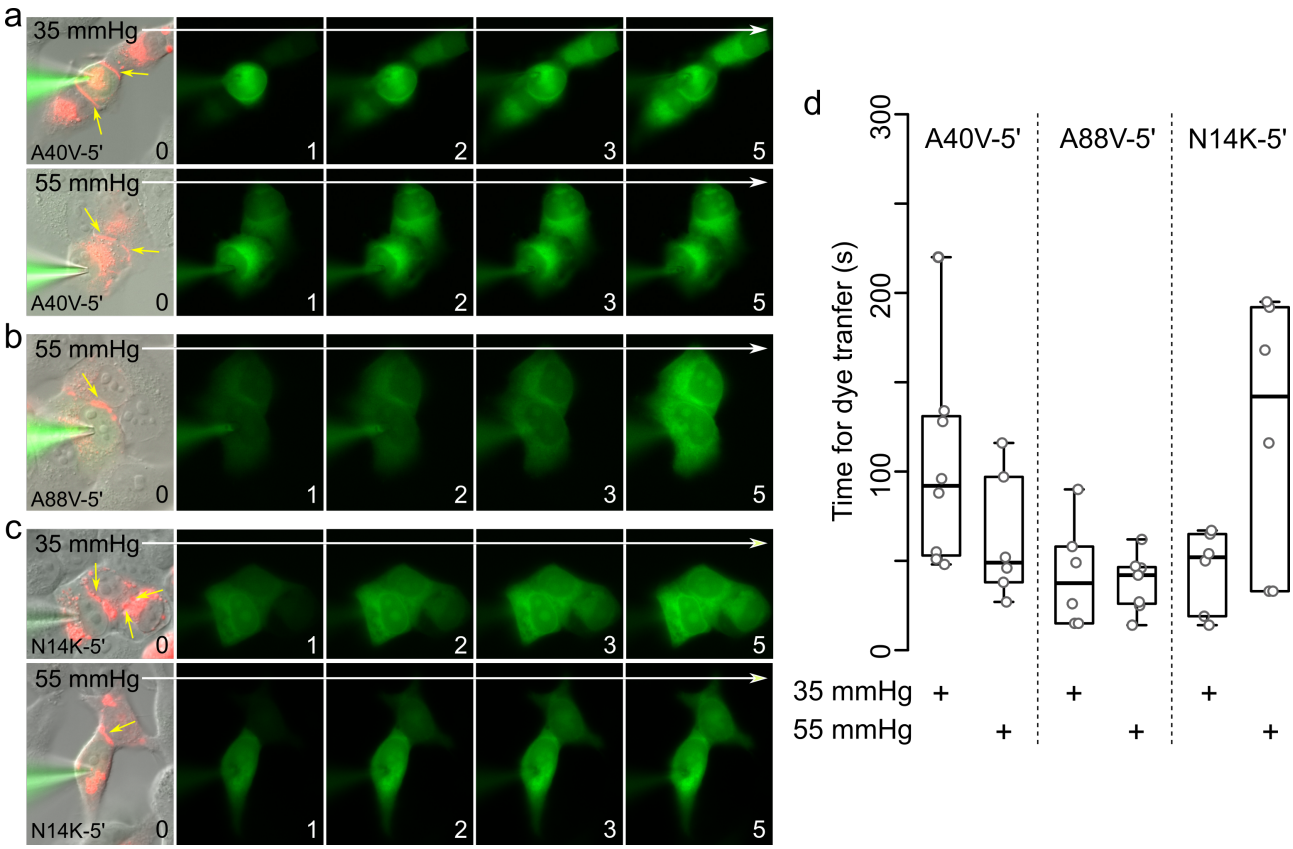

Figure 9. KIDS mutations of Cx26 alter the CO_2-sensitivity of Cx26 gap junctions. a) Gap junctions (indicated by yellow arrows) formed by $Cx26^{A40V-5'}$ (combining the A40V mutation with M151L, to eliminate alternative splicing) are highly permeable to NBDG and lack any CO_2 sensitivity. The images encompass 5 minutes of recording at a PCO_2 of 35 mmHg (top) and 55 mmHg (bottom). Permeation of NBDG to the coupled cells happens within 2 minutes in both conditions. b) Gap junctions (indicated by yellow arrows) formed by $Cx26^{A88V-5'}$ are insensitive to PCO_2 -rapid permeation occurs to the coupled cell even at a PCO_2 of 55 mmHg. c) Gap junctions formed by $Cx26^{N14K-5'}$ are not closed by CO_2. Permeation of NBDG is to coupled cells is shown at PCO_2 of 35 mmHg (top row) and 55 mmHg (bottom row). d) Summary data showing the time for dye transfer to the coupled cell. While A40V-5' and A88V-5' show no difference in permeation time with PCO_2, there is a tendency for the dye to permeate more slowly to the coupled cells for N14K-5'.

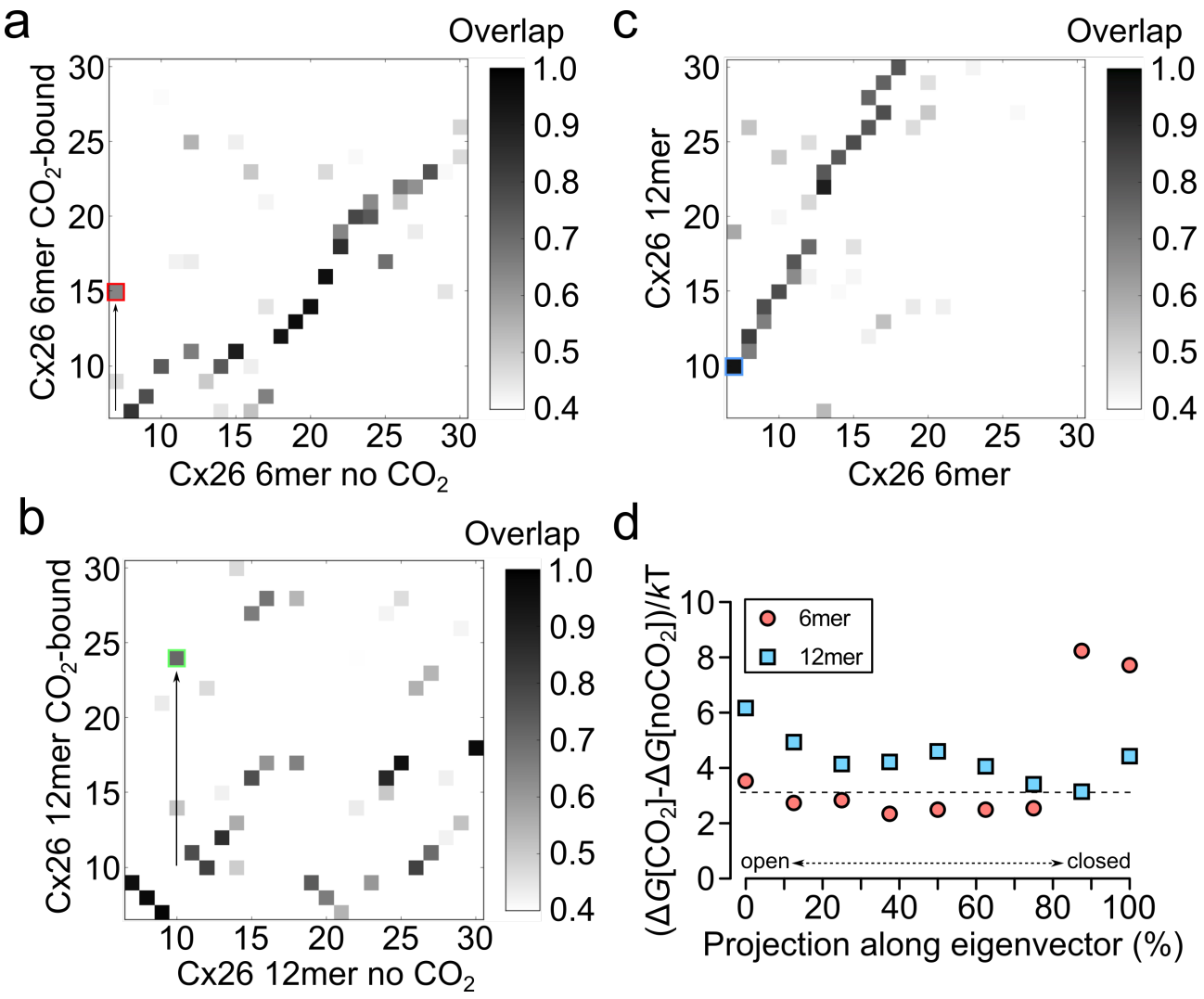

Figure 10. Analysis of the effect of CO_2 on Cx26 hemichannel and gap junction gating via elastic network modelling. a) The main open-close mode in the hemichannel (6mer) in the absence of CO_2 (mode 7) is reordered to mode 15 (red square) in the presence of CO_2. Therefore, this mode contributes less to the total motion of the molecule in the presence of CO_2 -the hemichannel spends more time open (Meigh et al., 2013). b) The main open-close mode in the gap junction (12mer) in the absence of CO_2 (mode 10) is reordered to mode 24 (green square) in the presence of CO_2. CO_2 thus reduces the contribution of this mode to the total motion of the molecule, but it is not possible to state whether the gap junction is predominantly in the closed or open state from this analysis alone. c) Correspondence of the modes for the hemichannel (6 mer) and gap junction (12 mer). Mode 7 in the hemichannel corresponds very closely to mode 10 in the gap junction (indicated by blue square). d) For a range of partially open and closed eigenvectors for both the hemichannel and the gap junction, we then calculated the change in free energy on CO_2-binding and thus the influence of CO_2 on the open/closed eigenvector. The closer the free energy value is to zero, the less energy needed to bind CO_2. The *x*-axis represents trajectory along the open/closed eigenvector going from

fully open to fully closed. The *y*-axis represents the free energy for binding CO_2 where the higher the value the less preferable is CO_2-binding. For the hemichannel, CO_2-binding is less energetically favourable in the closed state, whereas for the gap junction CO_2-binding is favoured in the closed state.